Quantifying the Mediterranean freshwater budget throughout the late Miocene: New implications for sapropel formation and the Messinian Salinity Crisis

Dirk Simon[a,*], Alice Marzocchi[b,c], Rachel Flecker[b], Daniel J. Lunt[b], Frits J. Hilgen[a], Paul Th. Meijer[a]

[a]*Department of Earth Sciences, Utrecht University, The Netherlands*
[b]*BRIDGE, School of Geographical Sciences and Cabot Institute, University of Bristol,BS8 1SS, United Kingdom*
[c]*Department of the Geophysical Sciences, The University of Chicago, USA*
*d.simon@uu.nl

Abstract

The cyclic sedimentary record of the late Miocene Mediterranean shows a clear transition from open marine to restricted conditions and finally to evaporitic environments associated with the Messinian Salinity Crisis. This evolution has been attributed to changes in Mediterranean-Atlantic connectivity and regional climate, which has a strong precessional pulse. 31 Coupled climate simulations with different orbital configurations have been combined in a regression model that *estimates* the evolution of the freshwater budget of the Mediterranean throughout the late Miocene. *The study suggests* that wetter conditions occur at precession minima and are enhanced at eccentricity maxima. We use the wetter peaks to predict synthetic sapropel records. Using these to retune two Mediterranean sediment successions *indicates* that the overall net freshwater budget is the most likely mechanism driving sapropel formation in the late Miocene. Our sapropel timing is offset from precession minima and boreal summer insolation maxima during low eccentricity if the present-day drainage configuration across North Africa is used. This phase offset is removed if at least 50% more water drained into the Mediterranean during the late Miocene, capturing additional North African monsoon precipitation, for example via the Chad-Eosahabi catchment in Libya. In contrast with the clear expression of precession and eccentricity in the model results, obliquity, which is visible in the sapropel record during minimum eccentricity, does not *have a strong signal in our model*. By exploring the freshwater evolution curve in a box model that also includes Mediterranean-Atlantic exchange, we are able, for the first time, to *estimate* the Mediterranean's salinity evolution, which *is quantitatively consistent with precessional control*. Additionally, we separate and quantify the distinct contributions regional climate and tectonic *restriction make* to the lithological changes associated with the Messinian Salinity Crisis. The novel methodology and results of this study have numerous potential applications to other regions and geological scenarios, as well as to astronomical tuning.

1. Introduction

At present, net evaporation and cooling increases the density of Mediterranean surface water, making it sink and ventilate the water column. This process of deep-water formation establishes a density gradient between the Mediterranean and the Atlantic, which drives anti-estuarine exchange at the Strait of Gibraltar (Rohling et al., 2015 and references therein). The Mediterranean sedimentary record demonstrates that this circulation pattern has not always been active. Atypical marine deposits occur in the form of organic-rich sediments (sapropels, Kidd et al., 1978), which populate the Mediterranean succession from the middle Miocene onwards (Rohling et al., 2015 and references therein), as well as by evaporites, which were precipitated during the Messinian Salinity Crisis (MSC; Roveri et al., 2014 and references therein). The occurrence of these anomalous sediments has been linked to changes in climate and Atlantic-Mediterranean connectivity. Sapropel formation is thought to occur due to stratification of the Mediterranean water column and enhanced surface productivity (e.g. Rohling et al., 2015 and references therein). These are generally considered to be related to a northward shift of the Intertropical Convergence Zone (ITCZ, Figure 1) during precession minima, when more North African monsoon rainwater contributes to the Mediterranean freshwater budget (Rossignol-Strick, 1983), but sapropels may also develop during rapid global sea-level fluctuations causing changes to the Mediterranean-Atlantic connectivity (e.g. Grant et al., 2016; Hennekam, 2015). The substantial volumes of Messinian gypsum and halite are indicative of a much higher Mediterranean salinity than today. Possible triggers for brine concentration consistent with evaporite precipitation include eustatic restriction of the Mediterranean connection with the global ocean, and/or tectonic changes in the gateway region (see Flecker et al., 2015), together with strong, net evaporative loss across the basin surface.

To date, neither the gateway evolution, nor the past Mediterranean freshwater budget evolution have been quantitatively constrained. Previous studies of the freshwater budget have either (1) assumed it was constant, and used the present day value (Blanc, 2000); (2) used a budget derived from a late Miocene idealized Atmospheric General Circulation Model (AGCM) simulation by Gladstone et al. (2007) (e.g. Simon and Meijer, 2015); (3) assumed that the freshwater budget is driven by fluvial discharge and changes linearly in phase with summer insolation at 65^{o}N (e.g. Hennekam, 2015); or (4) that fluvial discharge varies as an idealised sine function (Topper and Meijer, 2015). All these studies assume that changes in the freshwater budget control sedimentation (Ryan, 2008) and astronomical tuning uses this concept to date sedimentary successions with an accuracy on precession scale (e.g. Hilgen and Krijgsman, 1999).

Here, by contrast, we calculate a freshwater evolution for the Messinian (7.25-5.33 Ma) using a novel multi-model approach, which is based on fully coupled climate model simulations rather than on summer insolation at 65°N. This allows us to estimate the variation in precipitation (P), evaporation (E) and river discharge (R) throughout the Mediterranean region over the entire late Miocene and hence, to disentangle gateway and climate effects on the Mediterranean's environmental evolution for the first time. High temporal (~ 1 kyr) quantitative results are derived from an ocean-atmosphere-vegetation General Circulation Model (GCM; HadCM3L; Marzocchi et al., 2015). These GCM results are extended through time using a regression model (RM) to estimate the freshwater budget. *Assuming that a simple threshold value of the freshwater budget controls sediment type, we use the budget curve to calculate the pre-MSC sapropel pattern and compare it with late Miocene sapropel-bearing successions exposed in southern Spain (Abad composite, Sorbas, western Mediterranean) and Sicily (Falconara, central/eastern Mediterranean).* We also apply the curve to *an investigation of* the environmental changes that occurred at the onset of the MSC using a box model developed by Meijer (2006). Figure 2 illustrates how the various components of this study interconnect. *Our approach provides a new way to study the relationship between insolation, the Mediterranean freshwater budget and astronomical tuning. It provides new insights into the conditions under which sapropels and evaporites form and helps distinguish the* *role* of the Mediterranean freshwater budget in generating the region's environmental evolution from changes in Mediterranean-Atlantic connectivity.

2. Model hierarchy

2.1. General Circulation Model (GCM)

All numerical simulations are carried out using the UK Met Office General Circulation Model (HadCM3L version 4.5, see *Valdes et al., 2017 and references therein for a full description*), which is coupled to the TRIFFID vegetation model (Hughes et al., 2004 and references therein). This model has been previously used to simulate late Miocene (e.g. Marzocchi et al., 2015; Bradshaw et al., 2012) and Eocene (e.g. Tindall et al., 2010) climate. All our model simulations start from a 2000-years spin-up (Bradshaw et al., 2012), and are run for 200 years, which allows, at least, the atmospheric variables to be close to equilibrium and exhibit no significant trends (see Supplement in Marzocchi et al., 2015). In all simulations, CO_2 concentrations and the palaeogeography are fixed to the pre-industrial value of 280 ppm and to a late Miocene reconstruction derived from Markwick (2007), respectively. Each GCM experiment differs in the seasonal and latitudinal incoming solar radiation at the top of the atmosphere (hereafter, referred to as insolation). Insolation is determined by the orbital path and position of Earth relative to the Sun. The three most important orbital effects are (1) axial precession of the Earth, (2) the tilt of the Earth's rotational axis relative to its orbit (obliquity) and (3) the eccentricity of the elliptical Earth orbit around the Sun, with the Sun at one of the focal points. The orbital solutions of Laskar et al. (2004) determine how these orbital parameters changed through time for the Neogene period. The core of our GCM experiments (22 simulations) was carried out by Marzocchi et al. (2015) to study sub-precessional changes on the North African monsoon during the late Miocene. These 22 simulations (Figure 3C) are positioned at a relatively high eccentricity and spread not just across a whole precession cycle, but also from a maximum to a minimum obliquity (Figure 3). *In order to sample a wider range of orbital* *parameters, we ran additional simulations to gain more insight into the behaviour of the freshwater budget during low eccentricities (Figure 3B) and during the most extreme precession values for the period of interest (Figure 3A).*

2.2. Regression Model (RM)

2.2.1. Assessing the Mediterranean freshwater budget from the GCM

Precipitation, evaporation and runoff can be directly extracted from each grid box of the GCM. The annual mean runoff into the ocean is calculated following the method and river catchments defined by Gladstone et al. (2007). Each drainage basin shown in Figure 1 can be considered separately, so the impact of different combinations of basins draining into the Mediterranean at any specific time can be explored. While almost all the late Miocene river catchments resemble those that exist today (Figure 1), the prominent exceptions are the spatially extensive North African drainage basins that are currently dry (e.g. Chad- Eosahabi, Libya and Gabes; Figure 1). The sedimentary record in the Gulf of Sirt (Figure 1) is testament to a substantial fluvial system that drained the North African catchment west of the Nile from at least the Eocene, and continued to supply both water and sediment to the Mediterranean Sea during the late Miocene (Bowman, 2012). This is consistent with a more humid climate relative to today and an associated greening of the Sahel region (Colin et al., 2014). However, the southward extent of the Chad-Eosahabi drainage basin and its route across North Africa remain a matter of considerable debate, given that the palaeodrainage networks, which have been reconstructed using a variety of remote sensing techniques, are fragmentary as a result of being partly buried beneath aeolian sands. Griffin (2002, 2006) and Ghoneim et al. (2012) propose a fluvial link between Lake Mega-Chad and the Mediterranean, while Paillou et al. (2009) suggest that the rivers flowing into the Gulf of Sirt in the Miocene are instead likely to have drained north and east off the Tibesti Mountains, with a drainage divide between Chad and the Mediterranean. As Paillou et al. (2012) point out, there currently is insufficient evidence to confirm or refute a

Miocene connection between Lake Mega-Chad and the Mediterranean. This issue is critical for calculating the freshwater budget of the Mediterranean as the southward extent of these North African catchments dictates how much monsoonal precipitation can be transferred into the Mediterranean (Marzocchi et al., 2015; Bosmans et al., 2015a). In this study we have opted to model the largest possible drainage basin (Chad-Eosahabi; Figure 1) while acknowledging that in reality, the catchment and its resulting freshwater contribution to the Mediterranean may well have been significantly smaller. However, compared to proxy reconstructions indicating a greening of the Sahara during the mid-Holocene, most GCM simulations tend to underestimate the northward expansion (north of 21°N) of the summer monsoon (e.g. Pausata et al., 2016 and references therein). Consequently, we can assume that the intensified monsoonal rainfall in the late Miocene simulations of Marzocchi et al. (2015) could also be confined too far south in North Africa. Furthermore, Zhang et al. (2014) suggest that a greening of the Sahara would have occurred at every precession minimum from the late Miocene onwards.

Another important influence on the Miocene Mediterranean freshwater budget may have been the Paratethys, the lacustrine precursor of the Black and Caspian seas (Figure 1). New studies suggest that it was connected to the Mediterranean around 6.12 Ma (e.g. van Baak et al., 2015). Such a connection means that the Paratethys is both a potential water source (see de la Vara et al., 2016 for further discussion) and sink. The Paratethys has been implicated in hypotheses for several significant environmental phases of the MSC (Roveri et al., 2014): the Lago Mare phase (e.g. Marzocchi et al., 2016) and the Primary Lower Gypsum (PLG) deposition (Grothe, 2016). In contrast to the case of the Mediterranean, these Paratethys fluctuations are not precessional, but dominantly seasonal (Marzocchi et al., 2016). As we are considering annual changes, the freshwater input from the Paratethys is omitted.

2.2.2. Extending the GCM results via the RM

Typically, the influence of orbital parameters is evaluated through sensitivity tests of idealised extreme scenarios (e.g. Bosmans et al., 2015a; Tuenter et al., 2005). However, to calculate a continuous orbitally-driven evolution, it is important to (1) use age-specific orbital parameters (Laskar et al., 2004); (2) constrain climatic behaviour between orbital extremes; and (3) evaluate the system response to different orbital combinations over time (Laskar et al., 2004). Therefore the GCM simulations used here provide an excellent basis, as they cover a large range of orbital configurations. Visual comparison of the freshwater budget behaviour with summer insolation at 65°*N* through time suggests a temporal relationship between the two (Figure 3)*, with a clear anti-phase response of the freshwater budget to insolation. However, there is a* much more pronounced inflection towards higher ("wetter") values at insolation maxima (Figure 3C). This indicates that the evolution of the Mediterranean freshwater budget does not simply depend on summer insolation at 65°*N*, but must either be influenced by other factors or depend on a non-linear combination of the orbital parameters. Therefore, instead of linking the summer insolation curve at 65°*N* directly to the Mediterranean freshwater evolution (e.g. Hennekam, 2015), we calculate these freshwater values independent of the insolation target curve. To do so, we assume that the annual mean P, E and R depend on a linear combination of precession, obliquity, eccentricity, their squared terms and their cross-terms, giving a maximum of nine possible orbital terms (Equation 1*, 3 linear terms and 6 non-linear terms*). We then calculate a linear regression for each combination of these nine orbital parameters (using the package R, version 2.9; http://CRAN.R-project.org/package=leaps) and use a selection framework to identify the most appropriate regression equation amongst the large number of possible combinations For each regression with equal number of subset terms (one to nine), 10 combinations with the highest coefficients of determination (R^2) values above 0.9 are selected. By means of validation, their outcome is compared to three additional GCM experiments *(Figure 3C, 6.563 Ma, 6.594 Ma and for the present-day orbit)* that were not used to generate the regression.

The regression equation that predicts these simulations most closely is then used to calculate the late Miocene freshwater evolution of the Mediterranean *(see Equation 1 in combination with Table 1)*. The difference between the freshwater budget calculated by the additional GCM simulations and for the same orbits by the RM is used to estimate an uncertainty. This operation was performed five times to calculate different (combinations of) components of the freshwater budget: (1) precipitation minus evaporation (P-E) across the Mediterranean; (2) the rivers draining into the Mediterranean excluding the Chad-Eosahabi runoff (RnC); (3) the rivers draining into the Mediterranean including the Chad-Eosahabi runoff (RwC); and the net freshwater budget (4) without the Chad-Eosahabi basin (P-E+RnC); and (5) with the Chad-Eosahabi basin (P-E+RwC).

2.3. Applications of the freshwater budget evolution

This section describes examples of supplying the freshwater budget to a Mediterranean setting in which the sea-level was equal to that of the Atlantic. To consider a MSC desiccation scenario, reevaluation of the atmospheric convection patterns in a deep empty basin would be required (e.g. Murphy et al., 2009). In addition, evaporation is not considered as a function of sea-surface salinity because this is not expected to be of first-order importance.

2.3.1. Application I - Sapropel threshold analyses

The estimated freshwater budgets allow us to explore the relationships between Mediterranean sedimentation, runoff and freshwater budget for periods of Earth's history where the dating tools preclude high-resolution dating of individual horizons. Ideally, the RM would drive a biogeochemical model to evaluate sapropel formation. As a first pass, however, we used the simple threshold approach, which assumes that sapropel formation is directly proportional to freshwater input. This takes no account of sedimentation rate changes associated with productivity or the impacts of organic matter preservation or dilution, but does produce a synthetic sapropel log in the time domain, in a similar fashion as the pattern-matching of astronomical tuning. Four threshold analyses were carried out, for two runoff scenarios (RwC and RnC) and two net budgets (PERwC and PERnC). If the curves cross the prescribed threshold, which differs in each scenario, towards wet conditions, we assume a sapropel is deposited. The thresholds are kept constant and are chosen so that the number of predicted sapropels is as close as possible to that seen in the sedimentary record for the time period 6.6-6.0 Ma. The results are compared to the Abad composite (Sierro et al., 2001), an example of a marginal basin in the western Mediterranean and to the Falconara section (Hilgen and Krijgsman, 1999), an example of an intermediate depth basin in the central Mediterranean.

2.3.2. Application II - Box model analyses

Meijer (2006) adopted the notion that the Atlantic-Mediterranean exchange can be parameterized by letting the Mediterranean outflux vary in proportion with the salinity difference between the Atlantic and the Mediterranean. The constant of proportionality is the exchange coefficient, *g*. Using his one-box representation of the Mediterranean Sea, we calculate the Mediterranean salinity evolution for our net freshwater budget for three restricted scenarios. Prior to 6.7 Ma we set the gateway exchange efficiency to a value suitable for the modern Strait of Gibraltar (g ~10^6 (m^3/s)/(g/l)). From 6.7 Ma until 5.97 Ma a linear reduction in connectivity is imposed so that exchange efficiencies of 260, 1000 or 10000 (m^3/s)/(g/l) are achieved at the onset of the MSC (Manzi et al. 2013). Thereafter the exchange coefficient for each scenario is kept constant until 5.6 Ma, which marks the end of the PLG phase (Roveri et al. 2014). Both the freshwater budgets with Chad (PERwC) and without (PERnC) are considered.

3. Results

3.1. Quantifying the Mediterranean freshwater budget

The RM calculated coefficients are listed in Table 1. The five different freshwater budget combinations on the left can be calculated by summing up the products of the coefficients and the orbital curves calculated by Laskar et al. (2004):

$$freshwater\ budget = \sum_{1-10} coefficients * orbits$$

Figure 4 shows the freshwater budget evolution for the Messinian Stage (7.25-5.33 Ma). Whether the Chad-Eosahabi drainage is included or not, the annual mean freshwater budget of the Mediterranean is negative throughout the late Miocene. The freshwater budget does not simply depend linearly on the three orbital components (precession, obliquity and eccentricity): (1) the difference between evaporation and precipitation (E-P) across the whole basin varies +/- $0.5*10^{15}$ l/year about a value of around $-2.58*10^{15}$ l/year, (2) the two runoff curves (RnC, RwC) do not oscillate around a mean, but start from a base of around $2.5*10^{14}$ l/year and extend towards positive values (RnC ~$1.14*10^{15}$ l/year and RwC ~$2.96*10^{15}$ l/year) and (3) the strong and relatively constant difference in evaporation and precipitation causes the net freshwater budgets (PERnC, PERwC) to attain negative values with an oscillatory behaviour similar to the runoff curves.

Using the three additional and independent GCM simulations, we estimate an uncertainty of the RM results relative to the GCM results (Table 1). This uncertainty is of the order of ~10^{13} l/year, which is small relative to the budget variability of the order of 10^{15} l/year. Larger uncertainties (~10^{14} l/year) are found in the regressions including the Chad-Eosahabi drainage, as the positive freshwater excursions towards at insolation maxima are highly non-linear. Generally, this uncertainty is unlikely to cause large changes at eccentricity maxima, but may be more significant at low eccentricities due to the smaller amplitude of the freshwater budget. There is no evidence that this uncertainty affects the freshwater budget peak spacing.

The RwC regression equation sometimes shows negative excursions (e.g. 7.2-7.0 Ma and ~6.1 Ma). This is clearly a model artefact, since rivers can only add water to the Mediterranean, but cannot extract it. It develops due to the extremely non-linear nature of the freshwater budget around eccentricity maxima, where curve excursions to the negative are not very large, but excursions to the positive are significant. To counter this, when RwC < RnC we set RwC equal to RnC. *Nevertheless, this correction has no impact on the follow up analysis in this manuscript, because (1) peak spacing, (2) wet excursions, relevant for the threshold analyses (Section 3.2), and (3) net budgets, relevant for the MSC salinity evolution (Section 3.3), are all unaffected.*

The main periodicities lie around 20 kyr and are amplitude modulated by an approximately 100 kyr periodicity suggesting that the oscillations are dominantly precession and eccentricity related. Obliquity, which is visible in the Mediterranean sedimentary record at low eccentricities (Hilgen and Krijgsman, 1999; Lourens et al., 1996), is not manifest in the spectral analysis of the freshwater budget (see detailed discussion in Section 6).

The peak phasing of different freshwater budget curves relative to each other and to the astronomical curve, changes through time. While the two runoff curves (RwC and RnC) are in-phase with summer insolation at 65^{o}N throughout (Figure 4), the net freshwater evolution of P-E+RwC and P-E+RnC differ from each other, and peaks in these budgets are not always in-phase with insolation. Slight leads and lags characterise the entire period, but are more significant at the start and end of the Messinian (~7.2 Ma and ~5.3 Ma; Figure 4), and are opposite (out-of-phase) at ~6.1 Ma (Figure 4). The most likely cause of these phase offsets is the interaction of evaporation and precipitation over the Mediterranean and the rivers draining into it at times of low runoff. Although the runoff is dominated by north African rivers which are in phase with insolation, E-P is not always in phase with insolation.

3.2. Application I - A synthetic sapropel record

The runoff (RnC and RwC) and the net budget (PERwC) synthetics are in phase with insolation throughout, with the exception of the interval ~6.25 Ma where PERwC demonstrates a phase lag of half a cycle. The different phasing of the PERnC relative to insolation is particularly noticeable between 6.06–6.14 Ma, ~6.25 Ma and ~6.38 Ma. The duration of sapropels is predicted differently, depending on the freshwater curve used. The mean sedimentation rate of the Abad marls is approximately twice that of the Falconara section. This is due to the marginal character of the Sorbas basin compared to the more central deeper basin setting of Falconara. Despite this fact, the sedimentary changes follow a similar pattern.

If the sedimentation rate is assumed to be constant within a sapropel, our analyses predict thicker sapropels during eccentricity maxima and thinner sapropels during eccentricity minima. This is in agreement with field observations, but does not match with the observed precession-obliquity interference pattern (see detailed discussion in Section 6).

Another way to look at the problem is to retune the observed sapropels (Figure 5). We follow Sierro et al. (2001) and Manzi et al. (2013) in that we take the transition from the Abad composite to the Yesares Member to be continuous and tune downwards from the *Yesares Member (Abad) and the limestones (Falconara)*, respectively, by correlating midpoints of synthetics and observed sapropels. At ~6.35 Ma, an aberrantly thick whitish marl is present in the Abad composite, which encompasses the main sinistral to dextral coiling change of *N. acostaensis* (Sierro et al., 2001). The same coiling change is also found in the Falconara and Capodarso sections on Sicily (Hilgen and Krijgsman, 1999). However, these sections contain a very thin sapropel, which is missing in the Abad composite (marked “missing cycle” on Figure 5). Due to its weak expression and its very unusual position directly underlying a homogeneous marl, this sapropel is not taken into account when cycles were retuned to the freshwater budget curves.

The resulting sedimentation rates reveal variable distinct steps, which indicate abrupt changes in sedimentation rate:

1. At ~6.06 Ma the original double-peak insolation tuning to one sapropel introduces a phase shift between the original and all new tunings and consequently a change in the sedimentation rate. This offset is removed at ~6.14 Ma (PERnC) and ~6.16 Ma (PERwC), where both net budget curves predict one sapropel less. Although this introduces a small change in the age model, it provides an explanation for the double cycle assumption made in the original tuning.
2. At ~6.25 Ma, both (PERnC and PERwC) show diversions in the sedimentation rate from the original one. For PERwC this diversion only lasts for one cycle, because it is due to a long precession minimum translating into a wide insolation peak and a narrow freshwater peak. It demonstrates that sapropel midpoint tuning to orbital peaks needs to be reconsidered. For PERwC this diversion lasts longer, until ~6.4 Ma.
3. The offset in the oldest part of the section (older than 6.52 Ma) can be explained due to the simplicity of the threshold analyses and can be overcome by slightly lowering the threshold value used for PERwC.

This lets us conclude that the synthetics based on the net budgets (PERwC tuning being closest to insolation tuning) lead to an age model closest to the original one. Implications of this result are discussed in Section 4.

Although this procedure might be even more valuable for more recent times, our motivation and the setup of the GCM are specific for the late Miocene period. The Holocene sapropel record would be an interesting time frame to apply this method to, given the large amount of available data, but a full set of new numerical simulations would be required.

3.3. Application II - The MSC – salinity evolution

During the pre-restriction phase, the box model estimates Mediterranean salinity to be oscillating in parallel with the freshwater budget. Mediterranean salinity is slightly higher than (37.6-38.2 g/l, Figure 6B), but close to the prescribed Atlantic salinity of 36.5g/l, which is similar to today's Mediterranean situation (Rohling et al., 2015). With decreasing Atlantic exchange, the basin increases its sensitivity to freshwater oscillations greatly, and, irrespective of the freshwater budget used, Mediterranean salinity starts to rise, reaching concentrations suitable for gypsum concentration (e.g. 105 g/l, Grothe, 2016; 130 g/l Lugli et al. 2010 with a gateway efficiency of 260 $(m^3/s)/(g/l)$ (Figure 6A).

Between 5.97 Ma and 5.96 Ma our model predicts a sudden increase in salinity, which we interpret as the model expression of the Transitional Interval (Manzi et al., 2013). This interval is identified between the PLG and the pre-evaporite phase and contains a highly discontinuous gypsum bed (Manzi et al., 2013). Meijer (2012) already demonstrated that the increase in Mediterranean salinity is highly non-linear relative to the reduction in exchange so that even gradual restriction leads to sudden changes in the sedimentary record, as described by Kouwenhoven et al. (2003).

The extra freshwater from the Chad-Eosahabi catchment has two effects on Mediterranean salinity: (1) a slightly lower Mediterranean salinity for the same exchange coefficient and (2) more extreme salinity fluctuations in each precessional cycle (Figure 6B), driven by higher amplitude changes in the freshwater budget.

Figure 6C shows phase lags between the freshwater budget and the insolation curve. The greater the restriction of the Mediterranean from the global ocean, the longer the lag of the salinity peak behind the insolation minima (up to 5 ka) and of the salinity troughs behind insolation maxima (up to 2 ka, Figure 6C). This has already been demonstrated in the idealized model analysis of Topper and Meijer (2015) and again shows that we have to be careful in identifying tie points in the sedimentary succession.

4. Relevance for astronomical tuning and sapropel formation

In the Mediterranean, many Miocene and Plio-Quaternary sections have been astronomically tuned. To some extent, this tuning is based on the observation that cyclicity in the sedimentary succession mimics the insolation curve without clear identification of the processes that link insolation and lithology. Sapropel formation is linked to both productivity and stratification mechanisms and sapropels are assumed to form in-phase with summer insolation, given that a key driver of these mechanisms is thought to be fluvial discharge which is dominated by monsoon runoff (Rossignol-Strick, 1983). Consequently, the mid-point of sapropels is commonly used to tie Mediterranean successions to insolation maxima for astronomical tuning (e.g. Hilgen and Krijgsman, 1999). The temporal relationship between monsoonal runoff and insolation has been confirmed by transient modelling studies over the last 650 kyr (Weber and Tuenter, 2011), by a model investigation of a full Miocene precession/insolation cycle (Marzocchi et al., 2015; Marzocchi et al., 2016), and by idealized simulations (Bosmans et al., 2015b). Our calculated runoff evolutions also *indicate* in-phase agreement (Figure 4 and Figure 5), which provides additional support. The sapropel retuning to PERwC results clearly in the smoothest sedimentation rate curve (Figure 5). *We assume that the variable which gives the smoothest implied sedimentation curve, is the one most likely to control sedimentation (Occam's razor).* It is most similar to the sedimentation rate curve based on the original tuning to summer insolation 65°N. This holds for both sedimentary records shown in Figure 5. As they represent both the western and central Mediterranean these new insights are likely to be relevant for the entire Mediterranean basin. This indicates that the stratification and upwelling-induced productivity processes that lead to sapropel formation, are a function of the freshwater budget as a whole and not of fluvial discharge alone. Moreover, the importance of other contributors to the Mediterranean freshwater budget is illustrated by recent sapropels S1 and S5 both of which follow major deglaciations, and both of which lag insolation by ~3 kyr, either due to cold spells that interrupt the monsoonal intensification (Ziegler et al., 2010) or as a result of persistent meltwater pulses in the North Atlantic (Grant et al., 2016).

Faunal evidence (e.g. Kouwenhoven et al. 2003) suggests that the Late Miocene Mediterranean experienced salinity higher than today, already prior to the onset of the Primary Lower Gypsum. The interaction of increased freshwater input with this saltier, and therefore denser, water may have led to increased stratification, making stagnation of the basin more extreme and therefore potentially leading to sapropels at shallower water depths.

5. How much extra monsoonal runoff drains into the Mediterranean?

During the 400 kyr eccentricity minimum at ~6.1 Ma, Nile runoff alone is not sufficient to impose the temporal periodicity of its North African monsoonal precipitation on the net Mediterranean freshwater budget, because evaporation and precipitation across the Mediterranean are too strong (Figure 4 and Figure 7). This interaction of contributors to the P-E+RnC freshwater budget means that its peaks correspond well with insolation maxima at high eccentricities, but, at low eccentricities, it either fails to reach the sapropel threshold or predicts sapropel formation out-of-phase with insolation maxima. This phase-offset could mean that during the late Miocene more freshwater was supplied in-phase with precession. This extra water is parameterized in our model with the Chad-Eosahabi catchment. But, how much additional water volume is needed to match the phasing of the net freshwater budget and insolation and does it come from the Chad-Eosahabi basin? Reiterating that our synthetics are based on the assumption that sapropel formation is proportional to freshwater input (Section 2.3.2), we will tackle this question with Figure 7. Assuming that only the Nile catchment drains from North Africa into the Mediterranean, the maximum freshwater budget of this cycle occurs exactly at the insolation minimum rather than insolation maximum, which is when North African monsoonal precipitation is at its maximum. By gradually adding more freshwater, which we scale relative to the Chad-Eosahabi catchment (25%, 50% and 100%), an in-phase-peak with insolation can be generated. Figure 7 illustrates that approximately 50% more water volume than the maximum freshwater added by the Nile in the analysed time period is needed to match the freshwater budget peaks at the insolation minimum and maximum. To actually cause a significant effect, the volume needed is likely to be even larger. *It is important to realise that water flux and drainage basin size do not scale linearly so that we cannot directly infer from these results the size of Chad-Eosahabi basin during the Messinian.*

Another potential source of additional and precession-driven freshwater would be the Atlantic-Mediterranean winter storm tracks (e.g. Toucanne et al., 2015; Kutzbach et al., 2014), which may be especially significant for the western basin (Hoffmann et al., 2016). This contribution could be underestimated in the simulations of Marzocchi et al. (2015), as these indicate that the freshwater budget of the entire Mediterranean Sea would still be strongly dominated by summer monsoonal runoff into the eastern basin (Mayser et al., 2017, see their Figure 8).

Yet another precessional source that could potentially freshen the Mediterranean surface would be brackish Paratethys or 'fresher' Atlantic water. African runoff changes Mediterranean density in a cyclic fashion, as described in this study. This cyclicity is therefore likely to be found in the exchange strength of Mediterranean with its neighboring basins. Evidence outside the Mediterranean (e.g. Bahr et al., 2015) also hints at this process and forms an interesting objective for future work.

Due to the large volume of water needed to cause the phase-adjustment, we speculate that monsoonal-driven freshwater off the African continent is the most likely source. The route by which this freshwater reached the Mediterranean is difficult to be sure of. Because of the large volume required, it may have derived from Megalake Chad and drained via the Chad-Eosahabi river. Alternatively, it might have drained into the Mediterranean via the Nile or ephemeral wadi systems (see discussion in Coulthard et al., 2013) or via a combination of all three of these fluvial systems.

6. The precession-obliquity interference pattern

GCM experiments by Bosmans et al. (2015a) and Tuenter et al. (2005) conclude that both precession and obliquity influence African Monsoon precipitation and therefore runoff into the Mediterranean Sea. Bosmans et al. (2015b) recently suggested that the obliquity signal found in the Mediterranean sedimentary records (e.g. Lourens et al., 1996; Hilgen and Krijgsman 1999) can be explained by the low-latitude southern winter component in the insolation gradient that triggers cross-equatorial moisture transport and drives the North African monsoon. However, this conclusion only holds if the sedimentation rate is taken to be constant. The precipitation pattern across northern Africa from Bosmans et al.'s (2015a,b) idealised GCM experiments is very similar to that from Marzocchi et al. (2015) late Miocene runs. Both demonstrate an obliquity effect. *In addition, a recent study, that reconstructs the central North African rainfall record during the last glacial period (Hoffmann et al., 2016), suggests that obliquity played a role in positioning the ITCZ, however with different phasing than what was thought previously (e.g. Ziegler et al., 2010; Lourens et al., 1996).* Despite this, the freshwater hydrologic budget calculations for the Mediterranean GCM simulation (Figure 3) do not show an obliquity influence. Processes like precipitation depend on convection within the atmosphere, which occurs on sub-kilometer scale. As the spatial resolution of most GCMs is not high enough to capture convection, it is parameterised. The modern precipitation in the HadCM3 family of models (used here) has been assessed by Pope et al. (2011). The modern African monsoon seasonality in HadCM3 has been assessed by Marzocchi et al. (2015). Pope et al. (2011), as well as Marzocchi et al. (2015), found that it is in good agreement with observations. Dabang et al. (2005) assessed the accuracy with which a range of GCMs generated Asian monsoon precipitation, and found HadCM3 to be the best performing GCM. We are therefore confident that the GCM produces reliable results and discuss various possible reasons for the absence of an obliquity influence on the freshwater budget:

1. *One possibility is that the obliquity signal in the Mediterranean freshwater budget may be underestimated because of interactive vegetation feedbacks. While the simulations of Bosmans et al. (2015b) and Tuenter et al. (2005) had fixed vegetation, HadCM3L is coupled to a vegetation model in all orbital experiments used for the RM. In our simulations, the expansion of the tree fraction at times of enhanced North African monsoon would modify the soil's capacity to retain water (see Tuenter et al., (2005) for further discussion) and could reduce the water available to be transferred to the Mediterranean basin as runoff. In the sensitivity experiments by Bosmans et al. (2015b), a reduced tree fraction across North Africa (fixed to present day conditions) may allow more runoff into Mediterranean than the coupled model used by Marzocchi et al. (2015) and consequently the RM here.*
2. The catchment areas for North Africa differ slightly between Bosmans et al. (2015b; Figure 5) and Gladstone et al. (2007, see their Figure 1b) resulting in different runoff to the Mediterranean. However, comparison of more similar drainage basins suggests that small deviations in the African drainage basins will only play a minor role on the resulting Mediterranean runoff (not shown).
3. The precession-obliquity interference pattern in Mediterranean sapropels may also be explained by glacio-eustatic sea-level changes affecting Mediterranean-Atlantic connectivity. Such a connectivity change interacts with the *P-E+R* evolution to determine the biogeochemical response of the Mediterranean and hence the sedimentary succession formed. However, the obliquity signal in the Mediterranean's sedimentary record is found consistently throughout the Mediterranean's sapropel-bearing successions of the last 14 million years, while obliquity-induced glacial cycles occur only episodically and are most developed in the past 1 million years.
4. If obliquity has an effect on the African monsoon, this should be visible by comparing two simulations that have similar values for precession, but different obliquities. Such

experiments can be selected from Figure 3 with ages 6.568 Ma and 6.589 Ma, but these result in only minor differences in runoff. Comparing our results to Bosmans et al. (2015b) is difficult, as their idealized obliquity extreme experiments are run at zero eccentricity.

We conclude that obliquity does not influence North African-derived runoff to the Mediterranean sufficiently to cause a significant effect at eccentricity maxima. Additional HadCM3L experiments with zero precession and various eccentricity and obliquity values are needed to clarify this issue during eccentricity minima. *This suggests that care should be taken when interpreting our results during eccentricity minima.*

7. The onset of the MSC and the PLG stage

The focus of the box model study (Figure 6) is the onset of the MSC (5.971 Ma, Manzi et al., 2013), at which time the lithology changes from foraminiferal-bearing marls, to successions comprising alternations of evaporites and barren marls (Figure 5). Several authors have hypothesized that this change is due to a restriction in the gateway connectivity (e.g. Flecker et al., 2015). Figure 8 shows that even if the lower salinity threshold for gypsum precipitation is used (Grothe 2016), the gateway needs to be significantly more restricted than at present. The wider the gateway is, the stronger the effect of changing its depth. Even a relatively wide corridor of 15 km would need to shallow by at least 20 m to raise the basin salinity from present-day values to about 50 g/l (see Simon and Meijer, 2015 for further discussion on gateway dimensions). For narrower gateways and higher salinities, even more shallowing would be needed. Eustatic sea-level fall could be thought of as a possible mechanism for generating this gateway shallowing. However, the low resolution of the late Miocene benthic $\delta^{18}O$ record (e.g. Shackleton and Hall, 1997) makes it difficult to identify precessional or obliquity periods. Also, if restriction is sea-level related the salinity should decrease again during the time-span of the PLG. We conclude that although eustatic sea-level will affect some of the details of the Mediterranean salinity evolution, the actual onset of the MSC was driven by tectonics.

PLG deposits are well-preserved in the Mediterranean (Sorbas, Vena de Gesso, Sicily, Roveri et al., 2014). The 17 and 16 evaporite (gypsum) cycles in Italy and Spain, respectively, correspond well with each other and imply a total duration of approximately 350-370 kyr for the PLG (Roveri et al., 2014). This assumes the periodicity of the cycles is, like the pre-MSC marls, precessionally forced. Our modelled salinity evolution has 16 excursions towards fresher Mediterranean conditions and 16 or 17 higher salinity excursions (depending on whether the maximum at 5.6 Ma is counted, Figure 6A). The green threshold line (Figure 6A) illustrates how such salinity oscillations can oscillate in and out of a regime in which the Mediterranean reaches brine concentration suitable for precipitating gypsum (e.g. salinity concentration 130 g/l). Based on this example, the PLG salinity evolution can be matched to either of the hypotheses for gypsum formation e.g. saltier (Lugli et al., 2010) or fresher (Grothe, 2016), for different thresholds and can be linked to the observed number of gypsum cycles. This agrees with the previously used tuning assumption and quantitatively justifies, for the first time, that the PLG sediments are precessional-driven.

While we cannot use our results to identify whether the gypsum is linked to the dryer (Lugli et al., 2010) or wetter (Grothe, 2016) phases of the freshwater budget, we can argue that both scenarios benefit from having additional runoff from the Chad-Eosahabi basin: (1) If gypsum is in-phase with insolation minima (dryer and therefore saltier), the greater fluctuations in salinity mark a more defined distinction for moving in an out of the gypsum saturation concentration; (2) if gypsum is in-phase with insolation maxima (wetter and therefore fresher), greater monsoonal runoff from north Africa will prompt additional sulphate production in the Mediterranean, making gypsum precipitation more likely.

8. Conclusions

For the first time we have generated *an estimate of* the Mediterranean freshwater budget evolution throughout the late Miocene. This has been achieved via a novel multi-model technique by extending GCM results with a regression model and makes us conclude:

(1) Wetter climates occur during eccentricity maxima and precession minima, which is in good agreement with hypotheses for the Mediterranean sapropel-bearing sedimentary record. (2) At low eccentricities, differences can be identified in freshwater budget phasing due to differing E-P and R contribution through time. (3) When using the calculated synthetic sapropel record as a tuning target and comparing it to the original tuning we identify that the net freshwater budget is the most likely mechanism causing sapropel formation in the late Miocene. *This is best achieved with enhanced monsoonal runoff. These first three conclusions may be taken to endorse the existing paradigm for sapropel formation. (4)* As this additional runoff needs to be at least half the amount of the river Nile, we speculate that the Chad-Eosahabi supplied this enhanced discharge to the Mediterranean. *(5) Models differ in their sensitivity to obliquity with respect to the freshwater signal. Therefore, results at low eccentricity should be considered with care. Additional HadCM3L experiments with zero precession and various eccentricity and obliquity are required to investigate the obliquity effect on the African monsoon in greater detail. (6) Exploring our new freshwater budget evolution in a box model has shown that gypsum-marl cycles during the PLG are quantitatively consistent with precessional control.* (7) Greater monsoonal runoff from north Africa helps to explain the PLG observations. (8) Furthermore, our freshwater results allow us to disentangle the climatic and tectonic controls on Mediterranean environmental changes. We successfully demonstrate that the lithology change at the onset of the MSC can be linked to gateway restriction, which was most likely of tectonic nature.

Acknowledgements

DS thanks the BRIDGE group for its great hospitality during his time spent at the University of Bristol. All authors thank Natalie Lord and Michel Crucifix for valuable feedback at early stages of this work. *Joyce Bosmans,* Arjen Grothe, Rinus Wortel and the whole MEDGATE Team are thanked for the valuable discussions and insightful comments to this study. In addition, two anonymous reviewers are thanked for their valuable comments on the manuscript, and Heather Stoll is thanked for the editorial handling. Moreover thanks go to C & M Carto for editing all figures. The research leading to these results has received funding from the People Programme (Marie Curie Actions) of the European Unions Seventh Framework Programme FP7/2007-2013/ under REA Grant Agreement No. 290201 MEDGATE.

References

1. Bahr, A., Kaboth, S., Jiménez-Espejo, F.J., Sierro, F.J., Voelker, A.H.L., Lourens, L., Röhl, U., Reichart, G.J., Escutia, C., Hernández-Molina, F.J. and Pross, J., 2015. Persistent monsoonal forcing of Mediterranean Outflow Water dynamics during the late Pleistocene. *Geology*, *43*(11), pp.951-954.
2. Blanc, P.L., 2000. Of sills and straits: a quantitative assessment of the Messinian Salinity Crisis. *Deep Sea Research Part I: Oceanographic Research Papers*, *47*(8), pp.1429-1460.
3. Bosmans, J.H.C., Drijfhout, S.S., Tuenter, E., Hilgen, F.J., Lourens, L.J. and Rohling, E.J., 2015a. Precession and obliquity forcing of the freshwater budget over the Mediterranean. *Quaternary Science Reviews*, *123*, pp.16-30.
4. Bosmans, J.H.C., Hilgen, F.J., Tuenter, E. and Lourens, L.J., 2015b. Obliquity forcing of low-latitude climate. *Climate of the Past*, *11*(10), pp.1335-1346.
5. Bowman, S.A., 2012. A comprehensive review of the MSC facies and their origins in the offshore Sirt Basin, Libya. *Petroleum Geoscience*, *18*(4), pp.457-469.
6. Bradshaw, C., Lunt, D., Flecker, R., Salzmann, U., Pound, M., Haywood, A. and Eronen, J., 2012. The relative roles of CO2 and palaeogeography in determining Late Miocene climate: results from a terrestrial model-data comparison. *Climate of the Past*, *8*(2), pp.715-786.
7. Colin, C., Siani, G., Liu, Z., Blamart, D., Skonieczny, C., Zhao, Y., Bory, A., Frank, N., Duchamp-Alphonse, S., Thil, F. and Richter, T., 2014. Late Miocene to early Pliocene climate variability off NW Africa (ODP Site 659). *Palaeogeography, Palaeoclimatology, Palaeoecology*, *401*, pp.81-95.
8. Coulthard, T.J., Ramirez, J.A., Barton, N., Rogerson, M. and Brücher, T., 2013. Were rivers flowing across the Sahara during the last interglacial? Implications for human migration through Africa. *PloS one*, *8*(9), p.e74834.

9. Dabang, J., Huijun, W. and Xianmei, L., 2005. Evaluation of East Asian climatology as simulated by seven coupled models. *Advances in Atmospheric Sciences*, *22*(4), pp.479-495.

10. de la Vara, A., van Baak, C.G., Marzocchi, A., Grothe, A. and Meijer, P.T., 2016. Quantitative analysis of Paratethys sea level change during the Messinian Salinity Crisis. *Marine Geology*, *379*, pp.39-51.

11. Flecker, R., Krijgsman, W., Capella, W., de Castro Martíns, C., Dmitrieva, E., Mayser, J.P., Marzocchi, A., Modestu, S., Ochoa, D., Simon, D., Tulbure, M., van den Berg, B., van der Schee, M., de Lange, G., Ellam, R., Govers, R., Gutjahr, M., Hilgen, F., Kouwenhoven, T., Lofi, J., Meijer, P., Sierro, F.J., Bachiri, N., Barhoun, N., Alami, A.C., Chacon, B., Flores, J.A., Gregory, J., Howard, J., Lunt, D., Ochoa, M., Pancost, R., Vincent, S. and Yousfi, M.Z., 2015. Evolution of the Late Miocene Mediterranean–Atlantic gateways and their impact on regional and global environmental change. *Earth-Science Reviews*, *150*, pp.365-392.

12. Ghoneim, E., Benedetti, M. and El-Baz, F., 2012. An integrated remote sensing and GIS analysis of the Kufrah Paleoriver, Eastern Sahara. *Geomorphology*, *139*, pp.242-257.

13. Gladstone, R., Flecker, R., Valdes, P., Lunt, D. and Markwick, P., 2007. The Mediterranean hydrologic budget from a Late Miocene global climate simulation. *Palaeogeography, Palaeoclimatology, Palaeoecology*, *251*(2), pp.254-267.

14. Grant, K.M., Grimm, R., Mikolajewicz, U., Marino, G., Ziegler, M. and Rohling, E.J., 2016. The timing of Mediterranean sapropel deposition relative to insolation, sea-level and African monsoon changes. *Quaternary Science Reviews*, *140*, pp.125-141.

15. Griffin, D.L., 2002. Aridity and humidity: two aspects of the late Miocene climate of North Africa and the Mediterranean. *Palaeogeography, Palaeoclimatology, Palaeoecology*, *182*(1), pp.65-91.

16. Griffin, D.L., 2006. The late Neogene Sahabi rivers of the Sahara and their climatic and environmental implications for the Chad Basin. *Journal of the Geological Society*, *163*(6), pp.905-921.

17. Grothe, A., 2016. The Messinian Salinity Crisis: a Paratethyan perspective. (PhD Thesis, ISBN: 978-90-6266-427-6, Utrecht Studies in Earth Sciences 107).

18. Hennekam, R., 2015. High-frequency climate variability in the late Quaternary eastern Mediterranean: Associations of Nile discharge and basin overturning circulation dynamics (PhD Thesis, ISBN: 978-90-6266-390-3, Utrecht Studies in Earth Sciences 078).

19. Hilgen, F.J. and Krijgsman, W., 1999. Cyclostratigraphy and astrochronology of the Tripoli diatomite formation (pre-evaporite Messinian, Sicily, Italy). *Terra Nova-Oxford*, *11*(1), pp.16-22.

20. Hoffmann, D.L., Rogerson, M., Spötl, C., Luetscher, M., Vance, D., Osborne, A.H., Fello, N.M. and Moseley, G.E., 2016. Timing and causes of North African wet phases during the last glacial period and implications for modern human migration. *Scientific reports*, *6*.

21. Hughes, J.K., Valdes, P.J. and Betts, R.A., 2004. Dynamical properties of the TRIFFID dynamic global vegetation model. *Met office, Hadley Centre Tech. Note*, *56*, p.23.

22. Kidd, R.B., Cita, M.B. and Ryan, W.B., 1978. Stratigraphy of eastern Mediterranean sapropel sequences recovered during DSDP Leg 42A and their paleoenvironmental significance. *Initial Reports of the Deep Sea Drilling Project*, *42*(Part 1), pp.421-443.

23. Kouwenhoven, T.J., Hilgen, F.J. and Van der Zwaan, G.J., 2003. Late Tortonian–early Messinian stepwise disruption of the Mediterranean–Atlantic connections: constraints from benthic foraminiferal and geochemical data. *Palaeogeography, Palaeoclimatology, Palaeoecology*, *198*(3), pp.303-319.

24. Kutzbach, J.E., Chen, G., Cheng, H., Edwards, R.L. and Liu, Z., 2014. Potential role of winter rainfall in explaining increased moisture in the Mediterranean and Middle East

during periods of maximum orbitally-forced insolation seasonality. *Climate dynamics*, *42*(3-4), pp.1079-1095.

25. Laskar, J., Robutel, P., Joutel, F., Gastineau, M., Correia, A.C.M. and Levrard, B., 2004. A long-term numerical solution for the insolation quantities of the Earth. *Astronomy & Astrophysics*, *428*(1), pp.261-285.

26. Lourens, L.J., Antonarakou, A., Hilgen, F.J., Van Hoof, A.A.M., Vergnaud-Grazzini, C. and Zachariasse, W.J., 1996. Evaluation of the Plio-Pleistocene astronomical timescale. Paleoceanography, 11(4), pp. 391–413.

27. Lugli, S., Manzi, V., Roveri, M. and Schreiber, C.B., 2010. The Primary Lower Gypsum in the Mediterranean: a new facies interpretation for the first stage of the Messinian salinity crisis. *Palaeogeography, Palaeoclimatology, Palaeoecology*, *297*(1), pp.83-99.

28. Manzi, V., Gennari, R., Hilgen, F., Krijgsman, W., Lugli, S., Roveri, M. and Sierro, F.J., 2013. Age refinement of the Messinian salinity crisis onset in the Mediterranean. *Terra Nova*, *25*(4), pp.315-322.

29. Markwick, P.J., 2007. The palaeogeographic and palaeoclimatic significance of climate proxies for data-model comparisons. *Deep-time perspectives on climate change: marrying the signal from computer models and biological proxies*, pp.251-312.

30. Marzocchi, A., Lunt, D.J., Flecker, R., Bradshaw, C.D., Farnsworth, A. and Hilgen, F.J., 2015. Orbital control on late Miocene climate and the North African monsoon: insight from an ensemble of sub-precessional simulations. *Climate of the Past*, *11*(10), pp.1271-1295.

31. Marzocchi, A., Flecker, R., van Baak, C.G., Lunt, D.J. and Krijgsman, W., 2016. Mediterranean outflow pump: An alternative mechanism for the Lago-mare and the end of the Messinian Salinity Crisis. *Geology*, pp.G37646-1.

32. Mayser, J.P., Flecker, R., Marzocchi, A., Kouwenhoven, T.J., Lunt, D.J., Pancost, R.D., in press. Precession driven changes in terrestrial organic matter input to the Eastern

Mediterranean leading up to the Messinian Salinity Crisis. Earth Planetary Science Letters, 10.1016/j.epsl.2017.01.029

33. Meijer, P.T., 2006. A box model of the blocked-outflow scenario for the Messinian Salinity Crisis. *Earth and Planetary Science Letters*, *248*(1), pp.486-494.

34. Meijer, P.T., 2012. Hydraulic theory of sea straits applied to the onset of the Messinian Salinity Crisis. *Marine Geology*, *326*, pp.131-139.

35. Murphy, L.N., Kirk-Davidoff, D.B., Mahowald, N. and Otto-Bliesner, B.L., 2009. A numerical study of the climate response to lowered Mediterranean Sea level during the Messinian Salinity Crisis. *Palaeogeography, palaeoclimatology, palaeoecology*, *279*(1), pp.41-59.

36. Paillou, P., Schuster, M., Tooth, S., Farr, T., Rosenqvist, A., Lopez, S. and Malezieux, J.M., 2009. Mapping of a major paleodrainage system in eastern Libya using orbital imaging radar: the Kufrah River. *Earth and Planetary Science Letters*, *277*(3), pp.327-333.

37. Paillou, P., Tooth, S. and Lopez, S., 2012. The Kufrah paleodrainage system in Libya: A past connection to the Mediterranean Sea?. *Comptes Rendus Geoscience*, *344*(8), pp.406-414.

38. Pausata, F.S., Messori, G. and Zhang, Q., 2016. Impacts of dust reduction on the northward expansion of the African monsoon during the Green Sahara period. *Earth and Planetary Science Letters*, *434*, pp.298-307.

39. Pope, J.O., Collins, M., Haywood, A.M., Dowsett, H.J., Hunter, S.J., Lunt, D.J., Pickering, S.J. and Pound, M.J., 2011. Quantifying uncertainty in model predictions for the Pliocene (Plio-QUMP): initial results. *Palaeogeography, Palaeoclimatology, Palaeoecology*, *309*(1), pp.128-140.

40. Rohling, E.J., Marino, G. and Grant, K.M., 2015. Mediterranean climate and oceanography, and the periodic development of anoxic events (sapropels). *Earth-Science Reviews*, *143*, pp.62-97.

41. Rossignol-Strick, M., 1983. African monsoons, an immediate climate response to orbital insolation. *Nature*, *304*(5921), pp.46-49.

42. Roveri, M., Flecker, R., Krijgsman, W., Lofi, J., Lugli, S., Manzi, V., Sierro, F.J., Bertini, A., Camerlenghi, A., De Lange, G. and Govers, R., 2014. The Messinian Salinity Crisis: past and future of a great challenge for marine sciences. *Marine Geology*, *352*, pp.25-58.

43. Ryan, W.B., 2008. Modeling the magnitude and timing of evaporative drawdown during the Messinian salinity crisis. *Stratigraphy*, *5*(1), pp.227-243.

44. Shackleton, N. J. and Hall, M. A., 1997, The Late Miocene stable isotope record, Site 926, in *Proceedings of the Ocean Drilling Program, Scientific Results*, vol. 154, pp. 367–373, Ocean Drilling Program, College Station, TX.

45. Sierro, F.J., Hilgen, F.J., Krijgsman, W. and Flores, J.A., 2001. The Abad composite (SE Spain): a Messinian reference section for the Mediterranean and the APTS. *Palaeogeography, Palaeoclimatology, Palaeoecology*, *168*(1), pp.141-169.

46. Simon, D. and Meijer, P., 2015. Dimensions of the Atlantic–Mediterranean connection that caused the Messinian Salinity Crisis. *Marine Geology*, *364*, pp.53-64.

47. Tindall, J., Flecker, R., Valdes, P., Schmidt, D.N., Markwick, P. and Harris, J., 2010. Modelling the oxygen isotope distribution of ancient seawater using a coupled ocean–atmosphere GCM: implications for reconstructing early Eocene climate. *Earth and Planetary Science Letters*, *292*(3), pp.265-273.

48. Topper, R.P.M. and Meijer, P.T., 2015. The precessional phase lag of Messinian gypsum deposition in Mediterranean marginal basins. *Palaeogeography, Palaeoclimatology, Palaeoecology*, *417*, pp.6-16.

49. Toucanne, S., Minto'o, C.M.A., Fontanier, C., Bassetti, M.A., Jorry, S.J. and Jouet, G., 2015. Tracking rainfall in the northern Mediterranean borderlands during sapropel deposition. *Quaternary Science Reviews*, *129*, pp.178-195.

50. Tuenter, E., Weber, S.L., Hilgen, F.J., Lourens, L.J. and Ganopolski, A., 2005. Simulation of climate phase lags in response to precession and obliquity forcing and the role of vegetation. *Climate Dynamics*, *24*(2-3), pp.279-295.

51. Valdes, P.J., Armstrong, E., Badger, M.P., Bradshaw, C.D., Bragg, F., Davies-Barnard, T., Day, J.J., Farnsworth, A., Hopcroft, P.O., Kennedy, A.T. and Lord, N.S., The BRIDGE HadCM3 family of climate models: HadCM3@ Bristol v1. 0. *Geoscientific Model Development Discussions*, pp.Under-Review.

52. van Baak, C.G., Radionova, E.P., Golovina, L.A., Raffi, I., Kuiper, K.F., Vasiliev, I. and Krijgsman, W., 2015. Messinian events in the Black Sea. *Terra Nova*, *27*(6), pp.433-441.

53. Weber, S.L. and Tuenter, E., 2011. The impact of varying ice sheets and greenhouse gases on the intensity and timing of boreal summer monsoons. *Quaternary Science Reviews*, *30*(3), pp.469-479.

54. Zhang, Z., Ramstein, G., Schuster, M., Li, C., Contoux, C. and Yan, Q., 2014. Aridification of the Sahara desert caused by Tethys Sea shrinkage during the Late Miocene. *Nature*, *513*(7518), pp.401-404.

55. Ziegler, M., Tuenter, E. and Lourens, L.J., 2010. The precession phase of the boreal summer monsoon as viewed from the eastern Mediterranean (ODP Site 968). *Quaternary Science Reviews*, *29*(11), pp.1481-1490.

Figure Captions

Figure 1: Schematic palaeogeographic map of the Mediterranean region during the late Miocene, based on Markwick (2007). Indicated are rivers that drained or might have drained into the

Mediterranean during the late Miocene, their catchment areas (schematic, following Gladstone et al., 2007), the present-day northern hemisphere summer and winter Intertropical Convergence Zone (ITCZ) and relevant field sections/areas (red). On a side note, the position of the summer ITCZ plotted is approximately the position of the summer ITCZ at precession maxima and the winter ITCZ plotted is approximately the summer ITCZ at precession minima (Marzocchi et al., 2015). In the GCM the Atlantic Ocean has been disconnected to capture the restricted basin behavior of the Mediterranean Sea during the MSC.

Figure 2: This flow chart illustrates how our multi-model approach compares with other methods and data. Oscillations in the orbit of the Earth are used during astronomical tuning to date sediment successions to high accuracy. Our method (green): we feed Earth insolation, based on orbital parameters in a GCM, from which we extract the precipitation, evaporation and river runoff across the Mediterranean region. These snap-shot results are extended in time via a RM. Results (blue): resulting is the Mediterranean freshwater budget evolution. Applications (red): we can compare our results to the sedimentary record directly (e.g. with a threshold analysis) (I) and we use them to calculate the Mediterranean salinity evolution for a certain Atlantic - Mediterranean gateway (II).

Figure 3: Summary of the GCM results and their position in time relative to the orbits. Figure A-C illustrate different data groups: (A) the most extreme insolation during the late Miocene, (B) the 400-kyr minimum at ~6.52 Ma and (C) the eccentricity maximum at ~6.58 Ma (Marzocchi et al., 2015) and two of the leave-out experiments. The astronomical curves (precession, obliquity and eccentricity) are normalised and centered around zero. Plot D gives an overview where the orbits fed into the GCM stand in time during the late Miocene.

Figure 4: Result overview for the Messinian stage (7.25-5.33 Ma). Plotted are the overall Mediterranean run-off (RnC and RwC), the evaporation minus precipitation (E-P) and the net Mediterranean budget (P-E+RnC and P-E+RwC). On the left, summer insolation at 65N (Laskar et

al., 2004), P-0.5*T (Lourens et al., 1996) and SITIG (Bosmans et al., 2015b) are shown for reference. If RwC < RnC we set RwC equal to RnC.

Figure 5: Model-Data comparison for the pre-MSC Mediterranean sedimentary record (6.6-6.0 Ma). Left: the Abad composite (Sierro et al., 2001); right: the Falconara section (Hilgen and Krijgsman, 1999). We follow Sierro et al. (2001) and Manzi et al. (2013) that the transition from the Abad composite to the Yesares Member is continues. The freshwater budget curves (RnC, RwC, PERnC and PERwC) and their synthetics are used to retune these two sections. This tuning is done downwards from the Yesares Member and the limestones, respectively, by correlating midpoints of synthetics and observed sapropels. This results in four sedimentation rates for the Abad composite (left) and four sedimentation rates for the Falconara section (right). These sedimentation rates are compared to the sedimentation rates of the original tuning with summer insolation at 65N. Obliquity, precession and eccentricity are plotted in the bottom panel for reference.

Figure 6: A: Calculation of the Mediterranean salinity in a box model, following Meijer (2006), for the time period 6.1-5.6 Ma. Shown are the two net freshwater budget (PERnC and PERwC) and their salt concentration for 3 restriction scenarios. The green line illustrates a gypsum threshold scenario, where gypsum deposits at 130 g/l. B: Close-up of A for a time period prior to the MSC. C: Close-up of A for the time period 5.825-5.775 Ma to illustrate the importance of the salinity peaks lagging behind the insolation curve.

Figure 7: Close-up of the 6.125-6.105 Ma cycle. The black curve is summer insolation 65^{o}N (Laskar et al., 2004), which is plotted without an y-scale. The yellow curve is the evaporation minus precipitation across the whole Mediterranean basin. The red curve is the net freshwater budget of the Mediterranean plus a percentage fraction of the Chad-Eosahabi runoff (0%, solid; 25%, 50% and 100%, various dotted lines).

Figure 8: The restriction coefficients presented in Figure 6 are translated into gateway dimensions at the onset of the MSC, by combining the theory of Meijer (2006) and Meijer (2012).

Table 1: Overview of resulting coefficients to calculate an annual mean freshwater budget ($*10^{15}$ l/year) evolution for the entire Mediterranean. The rows present the five equations, where P is precipitation, E is evaporation, RwC are all rivers draining into the Mediterranean including the Chad-Eosahabi catchment and RnC are all rivers draining into the Mediterranean excluding the Chad-Eosahabi catchment. The columns are the 10 coefficients needed for the calculation, the R^2 value for each regression and an estimate of the budget uncertainty.

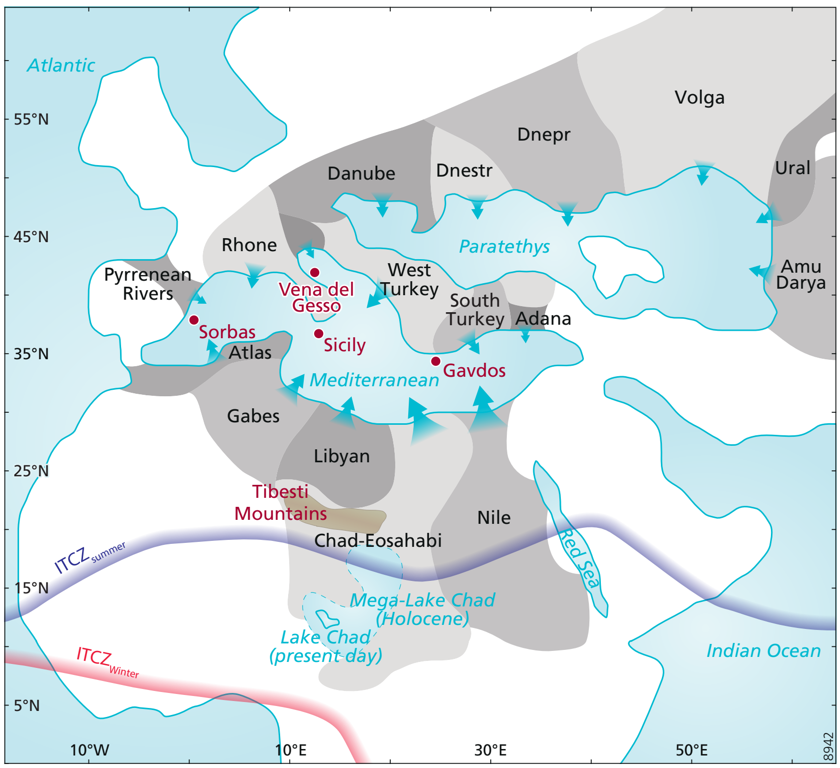

Atlantic
55°N
45°N
35°N
25°N
15°N
5°N
10°W
10°E
30°E
50°E
Volga
Dnepr
Danube
Dnestr
Ural
Paratethys
Rhone
Amu
Darya
Pyrrenean
Rivers
Vena del
Gesso
West
Turkey
South
Turkey
Adana
Sorbas
Sicily
Atlas
Gavdos
Mediterranean
Gabes
Libyan
Tibesti
Mountains
Nile
Chad-Eosahabi
Red Sea
ITCZ summer
Mega-Lake Chad
(Holocene)
Lake Chad
(present day)
ITCZ Winter
Indian Ocean
8942

Figure 1

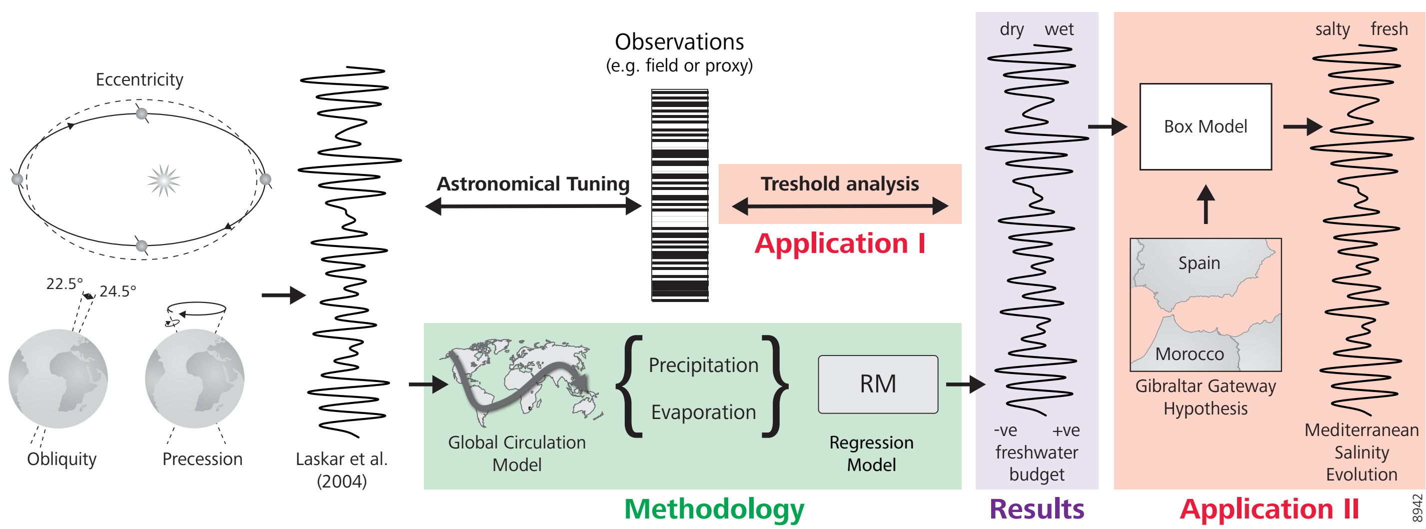
Eccentricity
22.5°
24.5°
Obliquity
Precession
Laskar et al. (2004)
Observations
(e.g. field or proxy)
Astronomical Tuning
Treshold analysis
Application I
Global Circulation Model
Precipitation
Evaporation
RM
Regression Model
Methodology
dry
wet
-ve
+ve
freshwater budget
Results
Box Model
Spain
Morocco
Gibraltar Gateway Hypothesis
salty
fresh
Mediterranean Salinity Evolution
Application II
8942

Figure 2

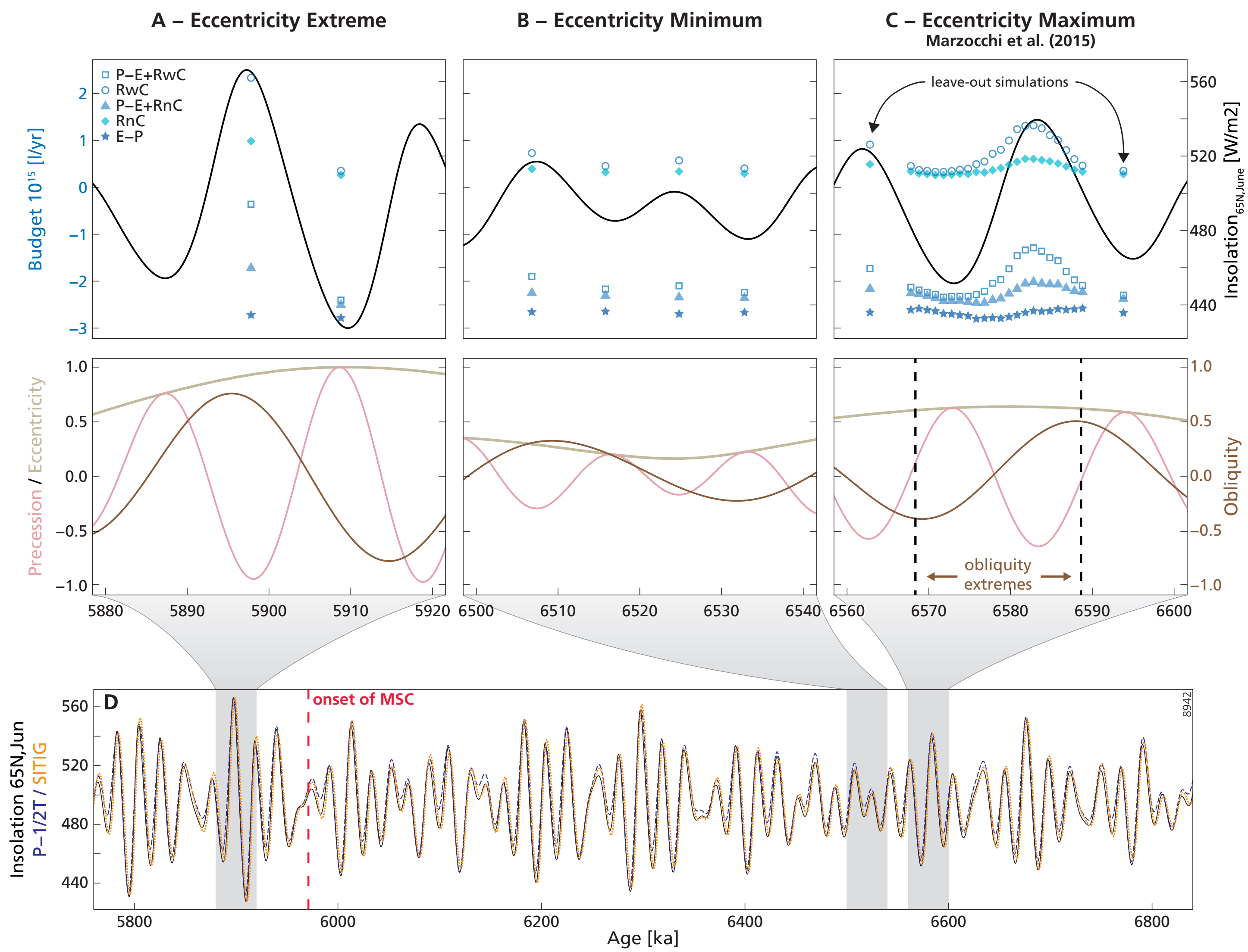

A – Eccentricity Extreme
B – Eccentricity Minimum
C – Eccentricity Maximum
Marzocchi et al. (2015)
P–E+RwC
RwC
P–E+RnC
RnC
E–P
Budget 10^{15} [l/yr]
leave-out simulations
Insolation$_{65N,June}$ [W/m2]
Precession / Eccentricity
Obliquity
obliquity extremes
D
onset of MSC
Insolation 65N,Jun
P–1/2T / SITIG
Age [ka]
8942

Figure 3

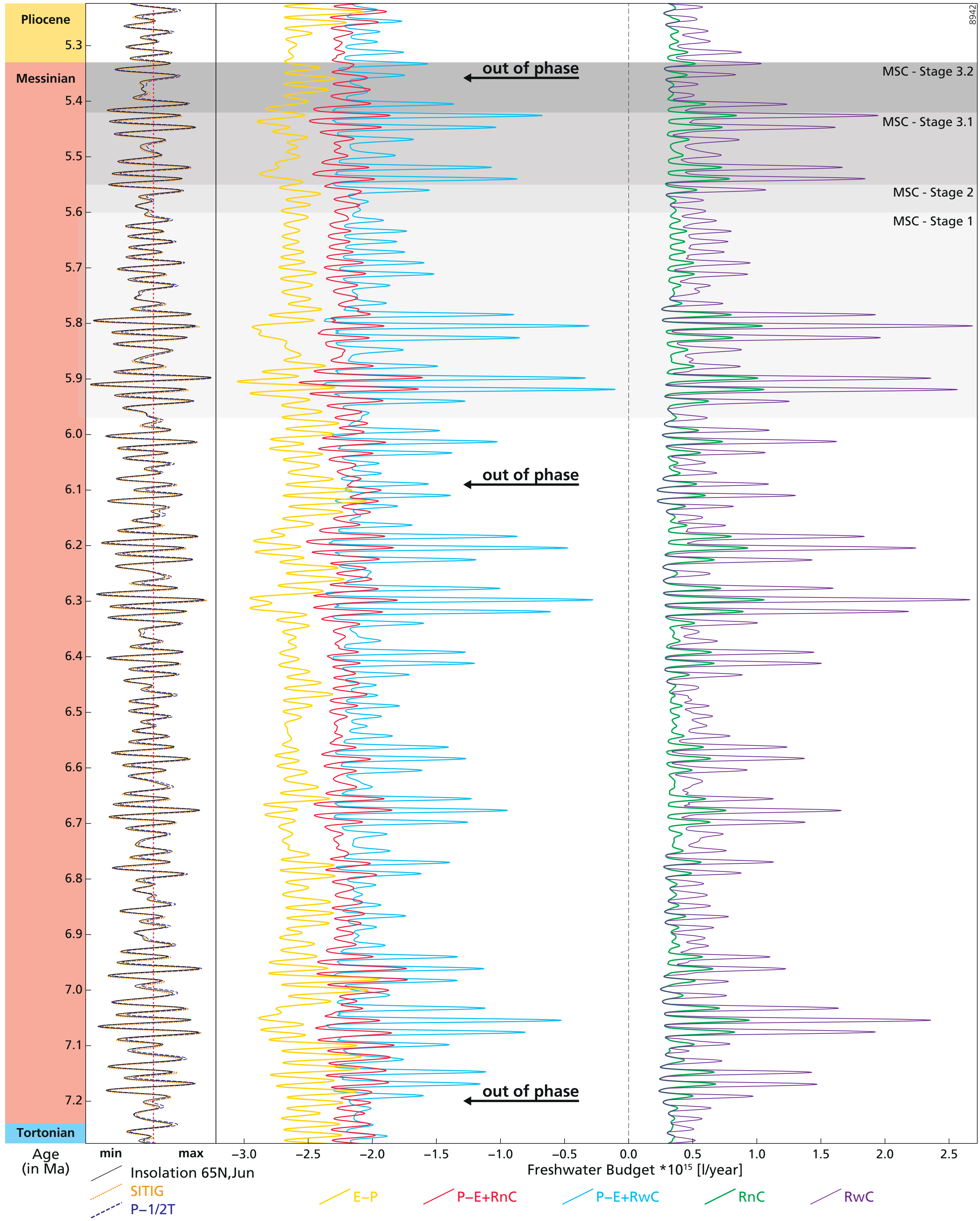

Pliocene
Messinian
Tortonian
out of phase
out of phase
out of phase
MSC - Stage 3.2
MSC - Stage 3.1
MSC - Stage 2
MSC - Stage 1
8942
Age
(in Ma)
5.3
5.4
5.5
5.6
5.7
5.8
5.9
6.0
6.1
6.2
6.3
6.4
6.5
6.6
6.7
6.8
6.9
7.0
7.1
7.2
min
max
−3.0
−2.5
−2.0
−1.5
−1.0
−0.5
0.0
0.5
1.0
1.5
2.0
2.5
Freshwater Budget *10^15 [l/year]
Insolation 65N,Jun
SITIG
P−1/2T
E−P
P−E+RnC
P−E+RwC
RnC
RwC

Figure 4

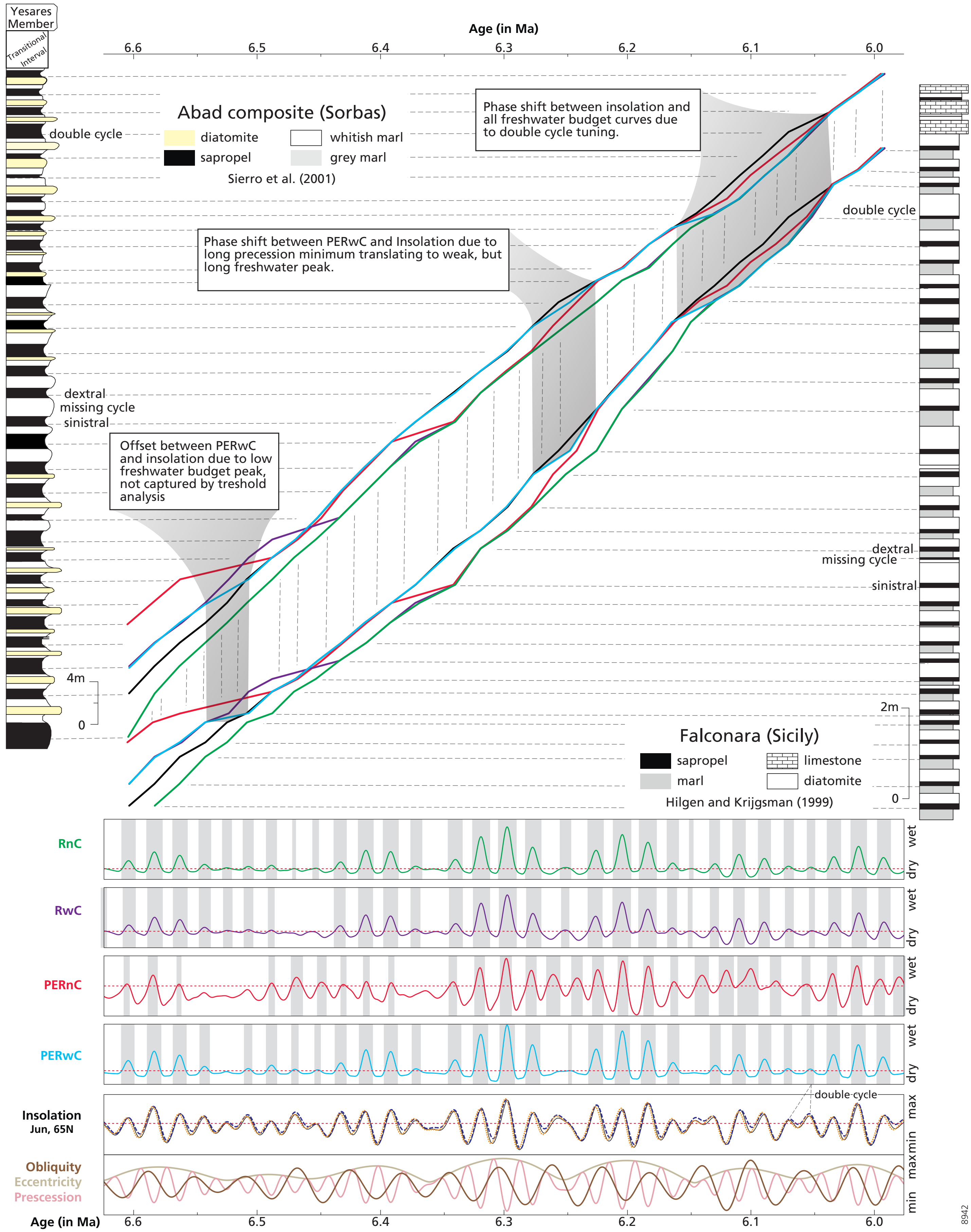
Yesares Member
Transitional Interval
Age (in Ma)
6.6
6.5
6.4
6.3
6.2
6.1
6.0
Abad composite (Sorbas)
diatomite
whitish marl
sapropel
grey marl
Sierro et al. (2001)
double cycle
Phase shift between insolation and all freshwater budget curves due to double cycle tuning.
Phase shift between PERwC and Insolation due to long precession minimum translating to weak, but long freshwater peak.
dextral
missing cycle
sinistral
Offset between PERwC and insolation due to low freshwater budget peak, not captured by treshold analysis
4m
0
2m
Falconara (Sicily)
sapropel
limestone
marl
diatomite
Hilgen and Krijgsman (1999)
RnC
RwC
PERnC
PERwC
Insolation
Jun, 65N
Obliquity
Eccentricity
Prescession
wet
dry
max
min
Age (in Ma)
8942
Figure 5

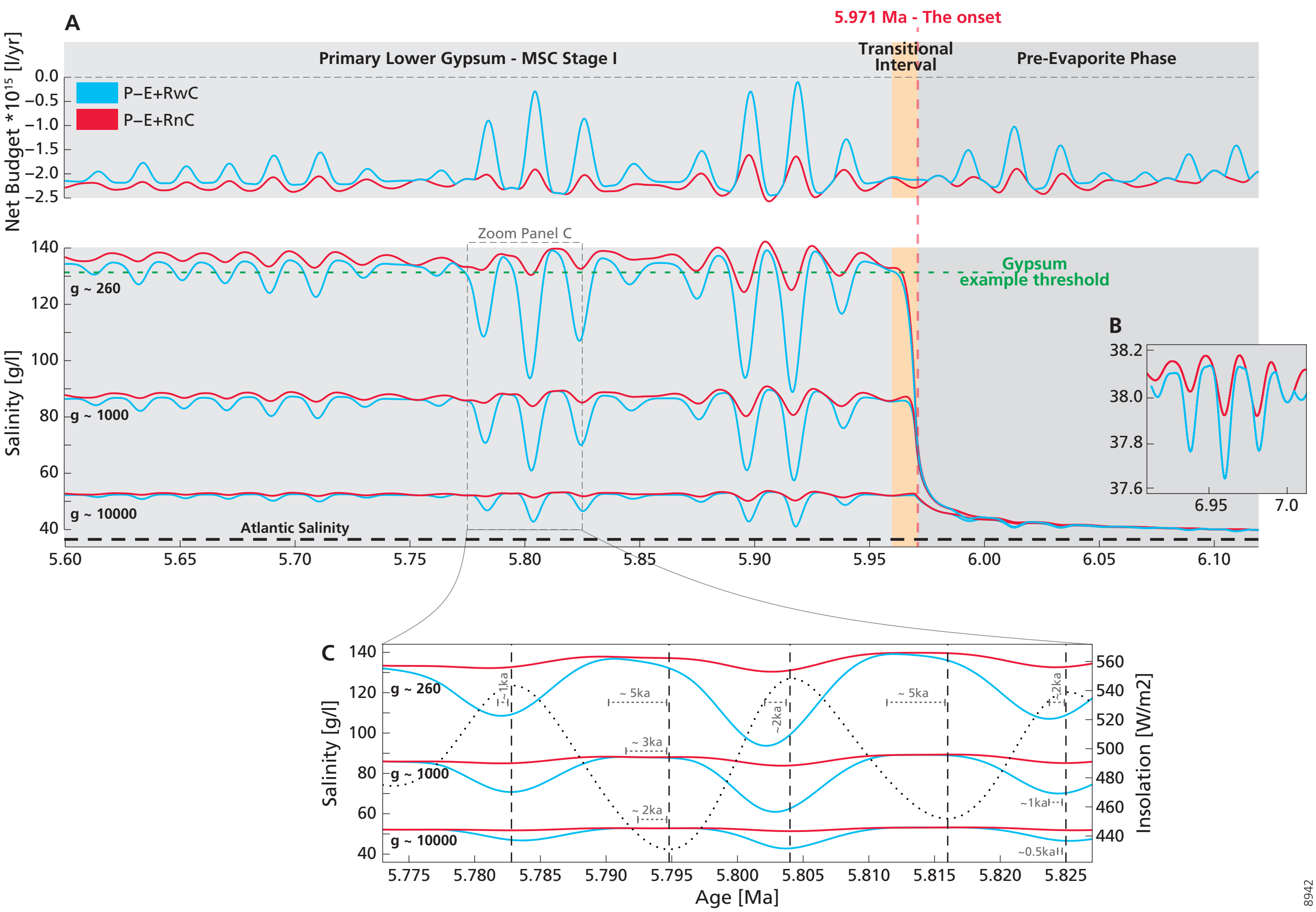

Figure 6

8942

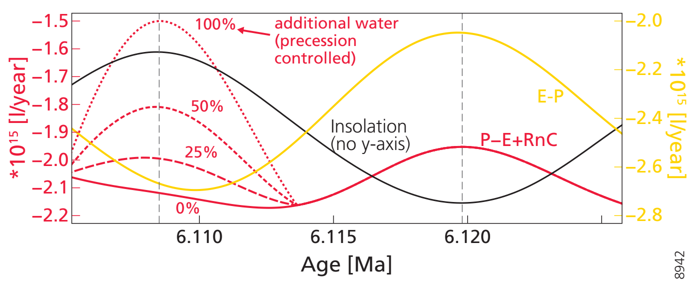
–1.5
–1.6
–1.7
–1.8
–1.9
–2.0
–2.1
–2.2
*10¹⁵ [l/year]
100%
additional water
(precession
controlled)
50%
25%
0%
Insolation
(no y-axis)
P–E+RnC
E-P
–2.0
–2.2
–2.4
–2.6
–2.8
*10¹⁵ [l/year]
6.110
6.115
6.120
Age [Ma]
8942

Figure 7

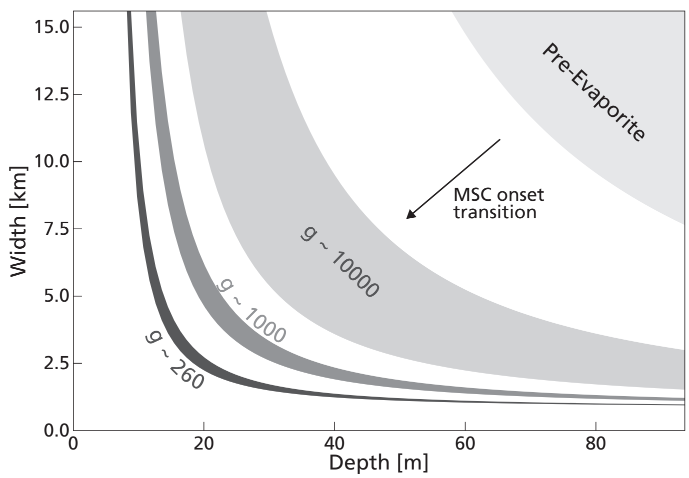
Pre-Evaporite
MSC onset
transition
g ~ 10000
g ~ 1000
g ~ 260
Width [km]
Depth [m]
15.0
12.5
10.0
7.5
5.0
2.5
0.0
0
20
40
60
80

Figure 8

Freshwater Budget	Intercept	Precession	Obliquity	Eccentricity	Precession^2	Obliquity^2	Eccentricity^2	Prec*Obl	Prec*Ecc	Obl*Ecc	R^2	Uncertainty
P-E+RwC	-2.142	0	0	0	0.665	0	0.256	0	-1.244	-0.071	*0.99*	$O(10^{14})$
P-E+RnC	-2.293	0	0	0	0.181	0.584	-0.109	0	-0.378	0	*0.96*	$O(10^{13})$
RwC	0.657	0	0.105	-0.713	0.616	-0.845	1.274	0	-1.252	-0.104	*0.99*	$O(10^{14})$
RnC	0.384	0	0.005	-0.211	0.201	-0.121	0.375	0	-0.421	0	*0.99*	$O(10^{13})$
P-E	-2.747	-0.079	0.131	0.484	0.004	0.863	-0.772	0	0.039	-0.396	*0.90*	$O(10^{13})$

Table 1 Overview of resulting coefficients to calculate an annual mean freshwater budget (*10^{15} l/year) evolution for the entire Mediterranean. The rows present the five equations, where P is precipitation, E is evaporation, RwC are all rivers draining into the Mediterranean including the Chad-Eosahabi catchment and RnC are all rivers draining into the Mediterranean excluding the Chad-Eosahabi catchment. The columns are the 10 coefficients needed for the calculation, the R^2 value for each regression and an estimate of the budget uncertainty.